Available online at www.sciencedirect.com

ScienceDirect

journal homepage: www.elsevier.com/locate/he

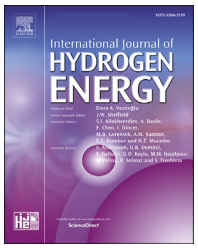

Advancing direct ethanol fuel cell operation at intermediate temperature by combining Nafion-hybrid electrolyte and well-alloyed PtSn/C electrocatalyst

Mauro André Dresch [a,1], *Bruno Ribeiro Matos* [a], *Denis Ricardo Martins Godoi* [b], *Marcelo Linardi* [a], *Fabio Coral Fonseca* [a], *Hebe de las Mercedes Villullas* [b], *Elisabete Inacio Santiago* [a,*]

[a] *Instituto de Pesquisas Energéticas e Nucleares, IPEN/CNEN-SP, Av. Prof. Lineu Prestes, 2242, 05508-000, São Paulo, SP, Brazil*

[b] *Instituto de Química, Universidade Estadual Paulista, UNESP, Rua Prof. Francisco Degni, 55, 14800-060 Araraquara, SP, Brazil*

HIGHLIGHTS

- Nafion-SiO_2 hybrids show improved hygroscopic properties and thermal stability.
- Hybrid with 6.5 wt% SiO_2 presents better proton conductivity than unmodified Nafion.
- Improved performance DEFC prototypes with Nafion-SiO_2 hybrid electrolytes.
- Substantial differences in DEFC performances depending on the PtSn/C anode catalysts.
- 112 mA cm^{-2} power density of 130 °C for 6.5 wt% SiO_2 hybrid and homemade PtSn/C.

ARTICLE INFO

Article history:
Received 6 October 2020
Received in revised form
12 January 2021
Accepted 19 January 2021
Available online 16 February 2021

Keywords:
Direct ethanol fuel cell
IT-DEFC
PtSn/C
Nafion-SiO_2
Hybrid electrolyte

ABSTRACT

The advancement of direct ethanol fuel cell (DEFC) represents a real challenge to electrochemical science because ethanol changes significantly the triple phase boundary properties such as the redox reactions and the proton transport. Ethanol molecules promote poor fuel cell performance due to their slow oxidation rate, reduction of the proton transport due to high affinity of ethanol by the membrane, and due to mixed potential when the ethanol molecules reach the cathode by crossover. DEFC performance has been improved by advances in the membranes, e.g., low ethanol crossover polymer composites, or electrode materials, e.g., binary/ternary catalysts. Herein, high temperature (130 °C) DEFC tests were systematically investigated by using optimized electrode and electrolyte materials: Nafion-SiO_2 hybrid electrolyte and well-alloyed PtSn/C electrocatalyst. By optimizing both the electrode and the electrolyte in conjunction, DEFCs operating at 130 °C exhibited a threefold increase on performance as compared to standard commercially available materials.

* *Corresponding author.*
E-mail addresses: elisabete.santiago@usp.br, eisantia@ipen.br (E.I. Santiago).
[1] Present address: Instituto de Ciências Naturais, Humanas e Sociais, Universidade Federal de Mato Grosso – UFMT, Av. Alexandre Ferronato, 1200–78550-728, Sinop, MT, Brazil.

https://doi.org/10.1016/j.ijhydene.2021.01.123

Introduction

PEM fuel cells directly fed with liquid fuels are regarded as a promising alternative to the current H_2-fed fuel cells mitigating the difficulty of H_2 storage and distribution. In this context, PEMFCs that use alcohols instead of H_2 as fuel, also called as Direct Alcohol Fuel Cells (DAFC), without the need of prior purifications, have been considered an emerging alternative power source for mobile and transportation applications [1].

Direct Ethanol Fuel Cells (DEFC) are particularly interesting because ethanol presents advantages over H_2 concerning storage and distribution, such as high theoretical power density, low toxicity, simple handling and availability [2]. Ethanol as fuel for electric vehicles is facilitated because it is a fuel largely used in internal combustion engines for vehicles in several countries having high energy density and a well-established infrastructure for production and distribution, which guarantees significant steps towards deployment of DEFC technology [3]. In addition, bioethanol, i.e. ethanol produced from bioprocesses via fermentation of various sources of biomass (beetroot, sugarcane, corn, etc.) [4], has a strong environmental appeal due to the potential reduction of CO, CO_2 and hydrocarbon-based pollutants [5,6]. Particularly, bioethanol produced from sugarcane - whose Brazil is the largest producer in the world [7] - is the biofuel with the most favourable energy balance. While typical emission from a gasoline internal combustion engine can reach ~200 g CO_2/km, a DEFC is expected to significantly decrease CO_2 emissions by one order of magnitude that is reabsorbed by the plant, making bioethanol a practically carbon-neutral fuel [8]. Such features categorize bioethanol as an economically viable and sustainable energy power source, and a promising protagonist in reducing of global warming impacts [9].

Unlike H_2 oxidation, the electrochemical oxidation of ethanol is a slow reaction that takes place through a complex mechanism involving parallel pathways [10]. In short, products of partial oxidation (acetaldehyde and acetic acid) are produced if ethanol is oxidized through a reaction path where the C–C bond is not broken (the so-called C2 pathway), while CO and CHx fragments that could be further oxidized to CO_2 are the reaction intermediates formed if scission of the C–C bond occurs (the so-called C1 pathway):

$$\text{C2 pathway: } CH_3CH_2OH \rightarrow CH_3CH_2OH_{(ad)} \rightarrow CH_3CHO \rightarrow CH_3COOH \quad (1)$$

$$\text{C1 pathway: } CH_3CH_2OH \rightarrow CH_3CH_2OH(ad) \rightarrow CO(ad), CHx(ad) \rightarrow CO_2 \quad (2)$$

The DEFC performance has been considered the main constraint on technology consolidation. Such feature is mainly associated with both sluggish ethanol electrooxidation kinetic and ethanol crossover effect. As cited above, the slow kinetic of ethanol electrooxidation is resulting from the difficulty of C–C bond cleavage by Pt-based electrocatalysts at low temperature (C2 pathway), causing large activation overpotential [11]. On the other hand, the crossover effect is related to the movement of ethanol from anode to cathode through the membrane, generating a mixed potential due to parallel and competitive oxygen reduction reaction (ORR) and ethanol oxidation reaction on cathode [12].

Increasing the operating temperature of PEMFC is highly desirable considering that at higher temperature (T~100–150 °C) electrochemical processes are kinetically favoured [13,14], and larger currents resulting from thermal activation of electrode reactions lead to improved cell performance. However, the operating temperature of PEMFC is typically limited to 80 °C. Such limitation imposed by state-of-the-art Nafion electrolytes is due to the strong dependence of the proton transport on the amount of water retained by the membrane. As the temperature is raised, the increase in the water vapor pressure decreases of the amount of liquid water in the polymeric membrane, which in turn rapidly decreases the proton conductivity of the electrolyte due to the reduction of proton charge carriers [15]. The need to keep such a delicate balance of the water content has motivated research efforts devoted to the development of alternative electrolytes composed by Nafion [16,17] or non-Nafion-based membranes [18–20], which combine satisfactory proton conduction and low permeability to ethanol fuel to allow high-performance DEFC operating above 100 °C.

Nanocomposites based on a polymeric membrane and hydrophilic oxides, such as TiO_2 [21,22] and SiO_2 [23,24], allow increasing the PEMFC operating temperature [25]. The physical retention of the water present in the oxide surface helps equilibrating the water loss on Nafion membranes when the operating temperature is increased [26–28]. In addition, the inorganic phase can act as a barrier that blocks the hydrophilic channels of the Nafion matrix physically preventing the crossing of the alcohol fuel to the cathode and reducing the effects of the mixed cathode potential with consequent improvement in the performance of DAFCs [29]. Among the oxides studied for the formation of organic-inorganic membranes, SiO_2 combines an increased water absorption capacity with the possibility of *in-situ* incorporation of tailored nanoparticles with average size that matches Nafion hydrophilic clusters (~4 nm) [30,31].

PtSn/C and PtRu/C have attracted considerable attention as electrode materials for DEFC. Electrocatalysts based on PtSn materials exhibit the highest activity towards ethanol oxidation reaction despite low efficiency in the conversion of ethanol to CO_2 [32,33]. It is well known that ethanol oxidation at low temperature takes place mainly through the C2 pathway. Additionally, several papers have shown that CO_2 yields are significantly lower for PtSn/C than for Pt/C at low temperature [34,35]. On the other hand, Pt/C and Pt-based bimetallic catalysts operating at high operating temperatures (~150 °C) showed a significant increase in the efficiency for the complete oxidation to CO_2 [36]. The key properties to reach high performance PtSn electrocatalysts can be controlled by the synthesis methodology. Particle sizes and structure, availability of Pt sites, degree of alloying and the amount of oxides play a major role to the electrocatalytic

activity [37,38]. Recently, Colmati et al. have reported the effect of both structural and electronic effects on PtSn/C-based anode toward ethanol oxidation. The authors have highlighted the importance of the presence of different Sn phases (intermetallic and oxides) in DEFC performance [39].

In general, the optimization of both components has been performed separately, i.e., the research papers are dedicated to either the electrolyte membrane or the electrode materials. Such approach resulted in limited improvements of the fuel cell performance since the electrode's redox reactions and the membrane proton transport are intricately mingled. Therefore, research efforts must be carried out in the pursuit of an understanding of the triple phase boundary improvements as a result of the advances made in the electrode and electrolyte materials. This investigation is even more necessary in DEFCs as the presence of a low dielectric constant solvent affects directly the kinetics of both charge transfer and proton transport.

In this study, we present experimental results evidencing that high performance DEFC operating at 130 °C can be achieved by combined properties of both the Nafion-SiO_2 hybrid electrolyte and active PtSn/C anode electrocatalyst. Our development has been focused on enabling the application of high-performance DEFC by the optimization of the main components responsible for irreversibility, i.e., electrodes and electrolyte. Anodes based on PtSn/C with low Pt loading (1 mg cm^{-2}) combined with Nafion-SiO_2 electrolytes that allow enhanced performance at 130 °C by accelerating the ethanol electro-oxidation and improving the conversion efficiency of ethanol to CO_2 are the main goal of this study. In this context, we show a significant improvement in DEFC performance by the optimization of physical-chemistry characteristics of anode and electrolyte for intermediate temperature (IT-DEFC), which represents a new approach to investigate the electrode/electrolyte performance DEFC performance.

Experimental

Preparation and characterization of Nafion-SiO_2 hybrids

Hybrids based on Nafion-SiO_2 were produced by *in-situ* SiO_2 incorporation into commercial Nafion 115 membranes (127 μm thickness, DuPont) via sol-gel reaction. Previously, Nafion membranes were treated in hydrogen peroxide solution (3% v/v) at 80 °C/1 h followed by rinsing with water at same conditions to remove organic traces. Subsequently, the membranes were treated with sulfuric acid solution (0.5 mol L^{-1}) at 80 °C/1 h providing Nafion-H^+-form membranes. The first synthesis step of the hybrids was the swelling of Nafion in isopropanol in a closed vessel for 30 min. In sequence, the silica precursor (Tetraethyl Orthosilicate – TEOS, Aldrich) was added to the reaction vessel where the membrane was kept for further 30 min. This part of the synthesis of the Nafion-SiO_2 hybrids was done with two different concentrations of TEOS (0.7 and 2.0 mol L^{-1}). In order to promote the acid-catalyzed hydrolysis reaction of TEOS, nitric acid (0.5 mol L^{-1}) was added and the system left to react at 50 °C for 30 min. The condensation reaction had taken place at 95 °C for 24 h in a vacuum oven. Finally, 0.5 mol L^{-1} H_2SO_4 treatment in the resulting hybrid membranes was conducted to eliminate precursors and unstable silica residues.

The silica incorporation as well as the water and ethanol uptake were gravimetrically determined using the following equation:

$$wt\% = \frac{M_S - M_D}{M_D} x100 \quad (3)$$

where, depending on the case, M_S is the weight of the Nafion-SiO_2 membrane and M_D is the weight of the unmodified Nafion membrane or M_S is the weight of the water or ethanol-saturated membrane (Nafion or Nafion-SiO_2 hybrid) and M_D is the weight of the dry membrane.

Differential scanning calorimetry experiments were conducted in a DSC Mettler Toledo calorimeter, model DSC 822. The DSC runs for water-saturated membranes were performed from 20 °C to 180 °C at 20 °C min^{-1} heating rate under N_2.

Proton conductivity measurements for Nafion and Nafion-SiO_2 hybrids were carried out in through-plane direction by using electrochemical impedance spectroscopy (EIS, Solartron 1260 Impedance/Gain-Phase Analyzer). The data were collected in the frequency range of 1 Hz to 1 MHz and *ac* amplitude of 100 mV in an optimized stainless-steel sample holder [40], consisting of a sample chamber and a water reservoir with independent temperature control. EIS measurements were performed at increasing temperature in the 40–130 °C range. For measurements at 100% relative humidity (RH), the sample chamber and the water reservoir were kept at the same temperature. With the purpose of evaluating the effect of ethanol on the proton conductivity, additional EIS measurements were carried out with the water reservoir filled with a 2.0 mol L^{-1} solution of ethanol in water, *i.e.,* the samples were in equilibrium with the vapor of the ethanol/water solution, which was achieved after 30 min of stabilization at each measured temperature.

Preparation and characterization of PtSn/C electrocatalysts

PtSn nanoparticles of nominal composition Pt:Sn 70:30 (in atoms) were initially obtained in a colloidal state by a polyol process using dioctyl ether as solvent with some modifications [41,42]. This process typically involves the use of a long-chain diol (1,2-hexadecanediol) as reducer and oleic acid and oleylamine as capping agents. The addition of lithium triethylborohydride allows having stronger reducing conditions. In brief, 1,2-hexadecanediol (Sigma-Aldrich, technical grade, 90%), platinum (II) acetylacetonate (Sigma-Aldrich, 97%) and tin (II) acetate (Sigma-Aldrich, 49.0–53.0 wt% Sn) were dissolved in dioctyl ether (Sigma-Aldrich, 99%). The mixture was heated under argon atmosphere up to 110 °C. At that temperature, the capping agents (oleic acid, Sigma-Aldrich, technical grade, 90% and oleylamine, Sigma-Aldrich, technical grade, 70%) were added. In sequence, the temperature was increased up to 220 °C and then an aliquot of solution of lithium triethylborohydride in tetrahydrofuran (Sigma-Aldrich, 1.0 M) was slowly added. The temperature of the reaction mixture was then raised until reflux (*ca.* 298 °C) and kept for 30 min to complete the reaction. Lastly, the system

was left to cool to room temperature. The PtSn nanoparticles were then separated and cleaned through a sequence of procedures involving flocculation by addition of ethanol, centrifugation and redispersion in hexane, which were repeated until obtaining a limpid solution as described elsewhere [41]. After the cleaning steps, the nanoparticles were supported on carbon powder (Vulcan XC-72, Cabot) by constant stirring in a mixture of hexane and isopropyl alcohol for 12 h. The nominal metal (Pt + Sn) loading was 20 wt%. The catalyst obtained was filtered, meticulously washed with ethanol, acetone, and water, and dried. All chemicals (Sigma-Aldrich) were utilized without further purification. The Vulcan XC-72 carbon powder was heat-treated at 850 °C in Ar atmosphere for 5 h before use.

Thermogravimetric analysis (TGA) was performed with a TA Instruments SDT 2960 equipment, under dynamic atmosphere of oxygen (100 mL min^{-1}), alumina crucible of 40 μL, α-Al_2O_3 as reference material, sample mass around 6 mg and heating rate of 10 °C min^{-1}. X-ray diffraction (XRD) measurements were carried out using a Rigaku Multiflex diffractometer, with an incident wavelength of 0.15406 nm (Cu Kα) and scan rate of 2° min^{-1}. Transmission electron microscopy (TEM) images were obtained in a Philips CM200 instrument operating at 200 kV. Some images were taken in scanning mode (STEM) with a FEI TECNAI G2 F20 HRTEM microscope. X-ray photoelectron spectroscopy (XPS) studies were performed with a commercial spectrometer (UNI-SPECS UHV), using the Mg Kα line (hν = 1253.6 eV) as the photon source and setting the analyzer pass energy to 10 eV.

DEFC tests

Catalyst layers of gas diffusion electrodes for single DEFC were prepared as described elsewhere [43]. A catalyst loading of 1.0 mg Pt cm^{-2} was used for both anode and cathode. The anode was based on PtSn/C (70:30–20 wt%) prepared by a modified polyol method, and commercial PtSn/C (75:25–20 wt %, BASF) for comparison. The cathode was composed by commercial Pt/C (20 wt%, BASF). In all cases, 30 wt% of Nafion ionomer was incorporated to the catalyst layer by using a Nafion solution (5 wt% in isopropanol, DuPont). The membrane-electrodes assemblies (MEA) were prepared by hot pressing of anode and cathode onto the membrane (Nafion-SiO_2 hybrid or commercial Nafion 115) at 125 °C and 1000 kgf cm^{-2} for 5 min.

DEFC polarization curves were carried out galvanostatically with a 5 cm^2 single cell with serpentine gas flow pattern. Before running ethanol curves, the fuel cells were activated with hydrogen and oxygen saturated by water at 80 °C and 3 atm at 0.7 V for 2 h. The single cell polarization curves were taken at 80 °C and 130 °C. Humified O_2 was heated at the same temperature of the fuel cell and back-pressured at 3 atm. The temperature of both the O_2 and the fuel cell was controlled independently by using resistances and type-K thermocouples. The DEFC was directly fed with 2.0 mol L^{-1} ethanol solution at room temperature (~25 °C) and flux was of 2 mL min^{-1}. Some experiments were also run with 2.0 mol L^{-1} solution ethanol flux of 5 and 10 mL min^{-1}. The experimental details of the experimental apparatus for DEFC tests are described in Fig. 1.

Results and discussion

Nafion-SiO_2 hybrid membranes

The amount of silica incorporated into the hybrid membranes and the uptake values for water and ethanol (2.0 mol L^{-1} and absolute) are given in Table 1, where the values for the unmodified Nafion 115 membrane are included for comparison. The results for the Nafion-SiO_2 hybrids show that increasing the TEOS concentration from 0.7 mol L^{-1} to 2.0 mol L^{-1} promoted a twofold increase of incorporated silica, from 6.5 wt% to 13 wt%. Both hybrids present higher water uptake as compared to unmodified Nafion. The water uptake values for Nafion-SiO_2 hybrids with different SiO_2 contents show a small variation. Data in Table 1 indicate that SiO_2 particles promote an increase in the water uptake but the increasing of inorganic particle fraction does not result in a proportional change in the water uptake. The uptake of ethanol solution for the hybrid membranes is higher than that of unmodified Nafion. As in the case of water uptake, the increase in ethanol solution uptake is not directly related to the amount of SiO_2 incorporated into the hybrid. The uptake of absolute ethanol increases with increasing SiO_2 content, reaching 120 wt% for the hybrid with 13 wt% SiO_2. In general, the results of Table 1 evidence the beneficial effects of silica incorporation, which can be ascribed to additional OH sites for water sorption provided by the silica particles. The increase in the ethanol uptake for hybrids reveals that the permeability of ethanol is not suppressed by the presence of SiO_2, which is in good agreement with previous report [28], where significant reduction in the ethanol uptake was observed for Nafion-TiO_2 hybrids with high fraction of TiO_2 (>10 wt%).

The thermal behavior of Nafion-SiO_2 hybrid membranes was studied by DSC measurements and results are shown in Fig. 2. For the unmodified Nafion sample (fully hydrated) a broad endothermic peak is observed at ~85 °C, which can be associated with different thermally activated processes occurring in the same temperature range, such as the α-transition, the ionomer crystallization and a significant loss of water [32,34,44]. Despite the larger water sorption values of the Nafion-SiO_2 samples, an appreciable shift to higher temperatures of the endothermic peak is observed for increasing inorganic content. As compared to Nafion, the temperature of the endothermic peak increases ~27 °C and 44 °C, for the hybrids with 6.5 wt% and 13 wt% SiO_2, respectively. The increase in temperature of thermal transitions observed for the hybrid membranes is likely related to the specific SiO_2 localization in the ionic domains of the polymeric matrix, as shown in previous reports [17,32,34]. The shift of thermal transitions towards higher temperatures depicted in Fig. 2 indicates that the silica nanoparticles act as a structural reinforcement of the Nafion polymeric matrix. A strengthened structure is crucial for the stability of hybrid electrolytes at high temperature in fuel cells [22].

Proton conductivity of Nafion and Nafion-SiO_2 hybrids measured in water and ethanol solution (2.0 mol L^{-1}) are depicted in Fig. 3. The experimental data show that proton conductivity displays a thermally activated behavior [40]. For measurements in equilibrium with water, all samples display similar temperature dependence of the proton conductivity,

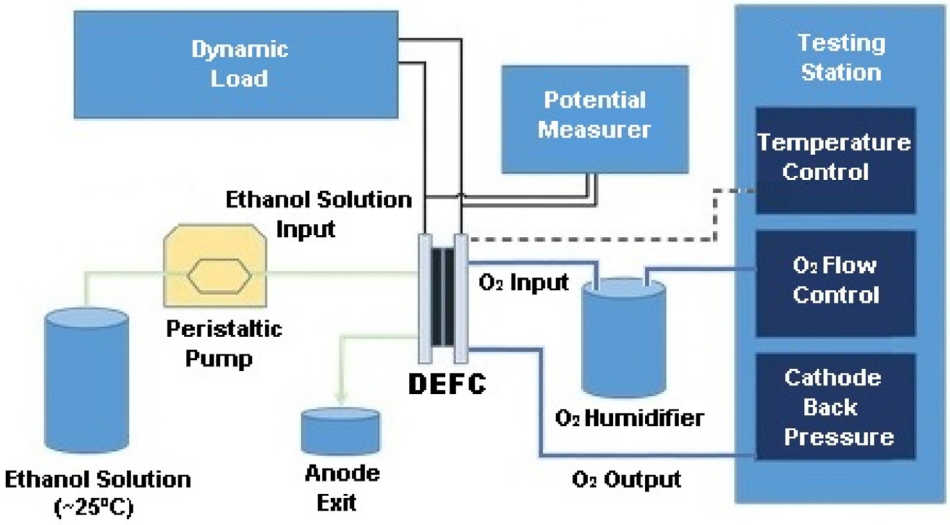

Fig. 1 – Schematic diagram of experimental apparatus for DEFC tests.

Table 1 – SiO_2 incorporation, uptakes for water, ethanol solution (2.0 mol L^{-1}) and absolute ethanol for Nafion and Nafion-SiO_2 hybrid membranes. All values are the average for three independent samples.

Sample	SiO_2 (wt.%)	Water (wt.%)	Ethanol (wt.%)	
			2.0 mol L^{-1}	Absolute
Nafion	–	30 ± 2	41 ± 4	92 ± 3
Nafion-SiO_2 (0.7 mol L^{-1} TEOS)	6.5 ± 2	38 ± 3	50 ± 3	110 ± 3
Nafion-SiO_2 (2.0 mol L^{-1} TEOS)	13 ± 2	40 ± 2	55 ± 4	120 ± 5

exhibiting an upturn for T > 90 °C. The Nafion-SiO_2 hybrid with 6.5 wt% SiO_2 shows the same conductivity of Nafion at low temperature. However, for T > 90 °C, the proton conductivity of hybrid sample surpasses that of Nafion. Such behavior can be attributed to the hygroscopic properties of SiO_2 particles, which retain more water at T > 90 °C, promoting better proton conductivity in this temperature range. The hybrid with 13 wt % SiO_2 displays lower conductivity in comparison with unmodified Nafion in the temperature range analyzed. This can be associated with the larger volume fraction of a less conducting phase (SiO_2) [28]. Nevertheless, such a decrease in conductivity is rather faint to produce a significant reduction in DEFC performance.

Fig. 3 shows a significant difference of the proton conductivity in ethanol solution as compared to the values obtained for the membranes in equilibrium with water. The proton conductivity measurements were obtained at the high frequency intercept of the impedance semicircle (~ 1 MHz). This high frequency intercept was recently ascribed to the proton conduction in nanometric length scales in the ionomer matrix [70]. Such high-frequency ac proton conductivity reflects the influence of the solvent on Nafion transport

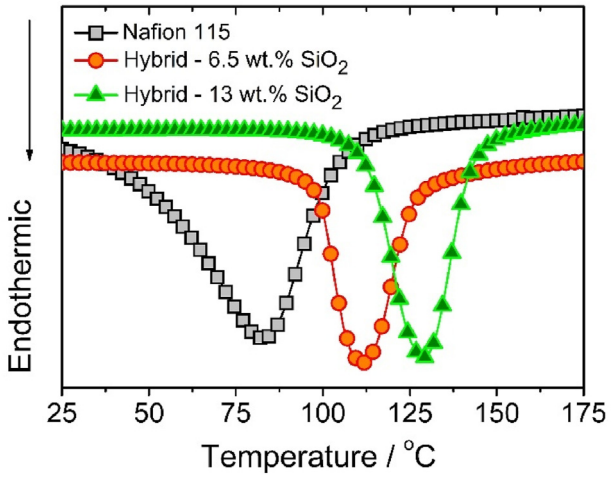

Fig. 2 – Differential scanning calorimetry curves for fully water-saturated Nafion and Nafion-SiO_2 hybrids.

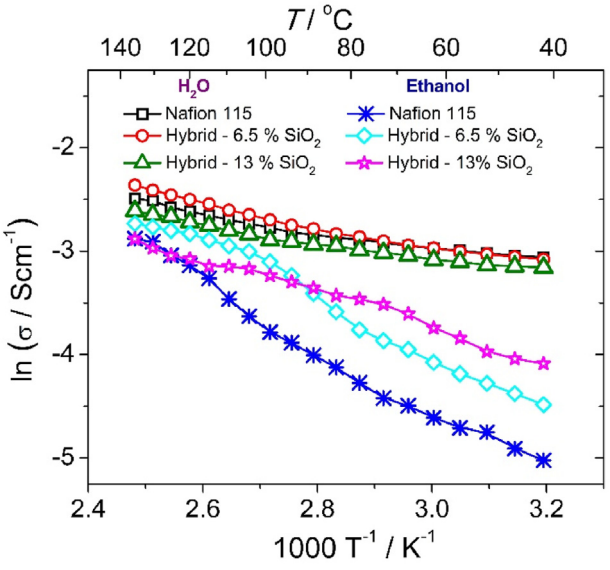

Fig. 3 – Arrhenius plots for Nafion and Nafion-SiO_2 hybrids in equilibrium with vapor of water and water/ethanol.

properties. At 40 °C, the Nafion conductivity equilibrated with water is 0.046 S cm^{-1}, whereas in equilibrium with ethanol solution the proton conductivity drops to 0.006 S cm^{-1}. Such a pronounced reduction is possibly related to: *i*) the lower proton transport rate in alcohol phase; and *ii*) the higher association of the protonic charges with the sulfonic acid groups due to the lower dielectric constant of ethanol. Measurements of proton conductivity of Nafion-SiO_2 samples in equilibrium with ethanol solution evidence different transport properties for the hybrids. A previous report showed that Nafion-SiO_2 prepared by casting, when in equilibrium with ethanol solution, has proton conductivities lower than Nafion [26]. In contrast, the hybrid membranes of this work have conductivities higher than that of Nafion in the 40–110 °C range.

The behavior of the proton conductivity of SiO_2 hybrids in ethanol is significantly less sensitive to the temperature increase than that of Nafion. The different thermally activated behavior of the conductivity in ethanol shows lower activation energies for hybrids membranes that suggest different proton transport mechanism as compared to Nafion. The proton conductivity of Nafion-SiO_2 hybrids in ethanol solution does not follow the Arrhenius (40–90 °C range) or Vogel-Tamman-Fulcher (90–180 °C range) behaviors, which prevents determination of the activation energy values [40]. The non-Arrhenius behavior might result, mainly, of the modulation of the charge transport with the motion of the main and side chains of the polymer, indicating that in a medium of lower dielectric constant the proton charges would be more coordinated with the polymer chain motion via interactions with the sulfonic acid groups. The increased mobility of the polymer chains by the interaction with ethanol molecules favors the proton transport. In this context, the stronger dependence of proton conductivity on the temperature of Nafion can be a result of the plasticization effects of solvent molecules [45].

In order to understand the proton conduction behavior of the hybrid membranes, it is important to consider that the ratio of evaporated water/ethanol binary mixtures is different from the water/ethanol ratio in the equilibrating solution [46]. The main reason is the higher rate of evaporation of the component with lower vapor pressure at the beginning of the evaporation process, resulting in a higher concentration of ethanol in the vapor phase. The complexity of this evaporation increases depending on the affinity of the binary mixture by the substrate. Nonionic polymer systems exhibit preferential wettability for the alcoholic phase [47]. Nafion displays affinity by both aqueous and alcoholic phases, which increases the complexity of the exact determination of the water/ethanol ratio into the film. Thus, the higher conductivity of the hybrids with respect to Nafion is possibly a result of the selective sorption of the hybrids, suggesting higher water content for the hybrid membranes. Moreover, proton conductivity is modulated by the mobility of the polymer chains, which, in turn, is affected by plasticization effects of solvent molecules [45]. The increased mobility of the polymer chains by the interaction with ethanol molecules would favor the proton transport. Another contribution to the higher conductivity of the hybrids in equilibrium with ethanol could come from the superficial proton conductivity of the SiO_2 phase due to water molecules strongly bound to the interface of sulfonic groups and/or SiO_2 nanoparticles.

PtSn/C catalysts

The metal loading of the in-house made PtSn/C catalyst was evaluated from TGA measurements carried out under oxygen atmosphere to eliminate the carbon support. A typical TGA curve is depicted in Fig. S1, which shows a small mass loss from *ca.* 130–400 °C, followed by an abrupt mass loss due to carbon oxidation. At ~480 °C, all carbon species were burned out, in accordance with previous data [48], and further increasing the temperature results in a constant value of the mass loss up to 800 °C. The determined mass loss value (20.5 wt%) is in good agreement with the nominal metal loading of the catalyst. However, it is reasonable to assume that the total mass loss includes some oxides resulting from metal oxidation on the catalyst surface, particularly Sn, in the as-prepared material as well as metal oxide formed at high temperature during the TGA run. It is also fairly unlikely that any further oxidation during TGA measurements would involve the whole particles. Nonetheless, possible variations of the mass loss due to such oxidized species represent minor variations in the metal loading because of the much higher atomic mass of the metal cations as compared to the that of oxygen. An estimate based on the amounts of oxides already present in the catalyst (see XPS results below) indicates that to reach a residual mass of 21% it would be necessary to oxidized 50% of all Pt atoms in the sample from Pt^0 to PtO_2. Thus, TGA results allow to conclude that the metal loading is very close to the nominal value of 20 wt%.

Fig. 4 shows the X-ray diffraction patterns of the homemade and commercial PtSn/C catalysts. The broad diffraction peak belonging to the [002] planes of graphitic carbon is seen at 2θ~25°. The remaining diffraction peaks are indexed as the Pt fcc structure (JCPDS 4–802), which are shifted to lower 2θ values compared to Pt, indicating PtSn alloying. Close inspection of the XRD data evidences that this shift is slightly larger for the homemade catalyst.

The diffraction peak of [220] Pt planes, which position and width at half-intensity were determined from the fitting of a pseudo-Voigt peak function, was used for calculations. The average crystallite size was calculated by Scherrer's equation (2.3 nm and 2.0 nm for homemade and commercial catalysts,

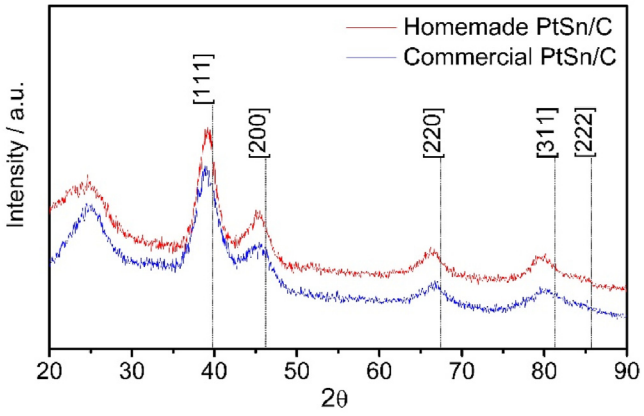

Fig. 4 – X-ray diffraction patterns for the homemade and commercial PtSn/C catalysts. Dotted lines indicate the signal positions for pure Pt.

respectively). The estimated the lattice parameters were 3.990 Å and 3.983 Å, for homemade and commercial samples, respectively.

The amount of Sn in the alloyed phase was calculated assuming that the PtSn system follows Vegard's law [49] up to 25 at.% Sn [50]. Thus, the Sn atomic fraction in the PtSn solid solution, x_{Sn}, was calculated as:

$$x_{Sn} = x_{alloy}\left(\frac{a_{Pt} - a_{sample}}{a_{Pt} - a_{alloy}}\right) \quad (4)$$

using as reference values the lattice parameter of the Pt_3Sn system (a_{alloy} = 4.00 Å) [51,52] and of commercial (E-TEK) Pt/C (a_{Pt} = 3.9155 Å) [53], and where x_{alloy} is the Sn atomic fraction (0.25) in the Pt_3Sn system [52]. From these calculations, the atomic composition of the PtSn alloy is Pt:Sn 78:22 and 80:20 for the homemade catalyst and the PtSn/C commercial sample, respectively.

A typical TEM image of the homemade PtSn/C catalyst and the distribution histogram of particle size are shown in Fig. 5. As it can be seen, the nanoparticles are uniformly dispersed on the carbon support, with the presence of few aggregates. The mean value of a Gaussian curve adjusted to the distribution histogram was used to estimate the average particle diameter, which turned out to be 2.7 ± 0.4 nm, in good agreement with crystallite size. Thus, the polydispersity index is σ = 0.15 [54]. For the commercial PtSn/C catalyst (Fig. S2), larger values of average particle size (3.4 ± 0.9 nm) and polydispersity index (σ = 0.27) were obtained.

The in-house made PtSn/C sample was analyzed by XPS. Fig. 6 shows the high-resolution XPS spectra of the Pt 4f and Sn $3d_{5/2}$ signals. In all cases, a Shirley background was used. For deconvolution, an asymmetric Doniach-Sunjic function [55,56] was used for metallic components and a mixed Gaussian-Lorentzian function for all non-metallic components. For the fitting procedure, the assymetry parameter (α_{DS}) was left to vary freely. In the case of Pt 4f, the spin-orbit splitting and intensity ratios between the 7/2 and 5/2 for each component were constrained to vary within 3% and 8% of the reported and theoretical values, respectively [55,57]. Additionally, the FWHM was constrained so that the two peaks of any doublet would have approximately the same value. The obtained assymetry values for Pt 4f and Sn 3d where α_{DS} = 0.2 and α_{DS} = 0.11, respectively, which agree well with reported values [57,58]. For Pt, 85% is Pt^0, while for Sn 38.7% is Sn^0, which indicates that Sn is mostly as oxide as usually found in the literature, although the material prepared in this work has a significantly higher content of metallic Sn as compared to other reports [59] indicating that the modified polyol synthesis provides the production of well-alloyed electrocatalysts.

To calculate atomic ratios, the corresponding sensitivity factors were used. For Sn 3d, the total area of the 3d doublet was calculated from the obtained area of the $3d_{5/2}$, using the theoretical value of intensity ratios [55]. The calculated Pt:Sn metallic atomic ratio, *i.e.* Pt^0 and Sn^0, is 83:17. Such value is slightly higher than that calculated by Vegard's law (Pt:Sn = 78:22) for the bulk alloy, possibly reflecting the presence of SnO_2 at the probed surface of the catalyst. Nevertheless, if the total amount of Pt and Sn (both metallic and non metallic) is considered, the Pt:Sn atomic ratio obtained is 68:32, in excellent agreement with the nominal composition (70:30). It is important to keep in mind that the atomic ratios between Pt and Sn might sligthly overestimate Pt content, since for a fixed photon energy Pt 4f, photoelectrons have a higher kinetic energy, thus having a larger probing depth than for Sn 3d (see Table 2).

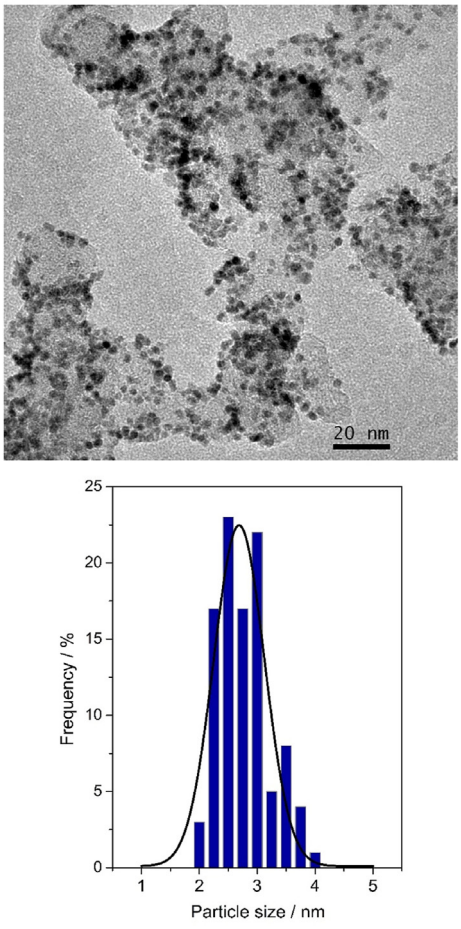

Fig. 5 – TEM micrograph for the homemade PtSn/C catalyst and distribution histogram of particle size.

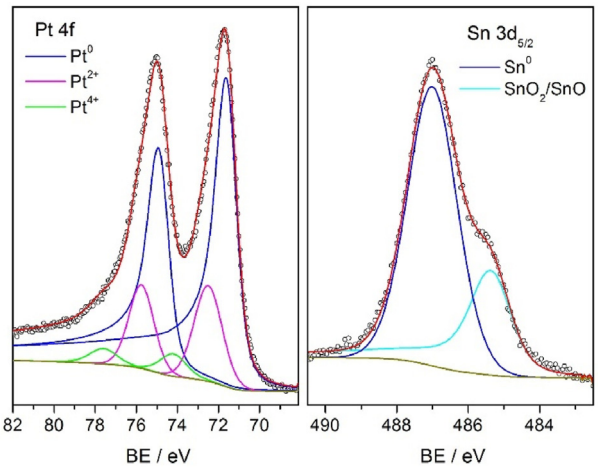

Fig. 6 – Pt 4f and Sn $3d_{5/2}$ XPS spectra for the homemade PtSn/C catalyst.

DEFC measurements

The unmodified Nafion 115 membrane and Nafion-SiO_2 hybrids were evaluated on DEFC at 80 °C and 130 °C with PtSn/C as anode catalyst. Polarization curves (*I*–*V*) obtained for Nafion 115 and commercial PtSn/C are depicted in Fig. 7. The increase in operating temperature had no practical impact on DEFC performance. The maximum power densities at 80 °C and 130 °C were 31 and 35 mW cm^{-2}, respectively. These values are quite similar to previously reported data for DEFC with Nafion 115 and commercial Pt_3Sn/C anode catalyst [53,60,61].

The open circuit voltage (OCV) is also an important parameter because it can be considered an indicative of fuel crossover response, *i.e.*, of the quantity of fuel that diffuses from the anode to the cathode through the electrolyte. Ethanol crossover through Nafion-based membranes results in a remarkable decrease on cathodic potential and, consequently, on cell potential. On the other hand, considering the lowering of the Gibbs energy as temperature is raised, a decrease in the OCV values at 130 °C would be expected [62]. However, the opposite effect was observed in OCV for DEFC operating at 130 °C in all DEFC experiments carried out in this study. The apparent improvement in the OCV might be associated with a slight suppression of crossover for the DEFC operating at 130 °C most likely due to the increase in the ethanol oxidation rate, which would reduce the amount of ethanol that can cross to the cathode compartment. Moreover, the OCV improvement might be partially compensated by a more pronounced ohmic polarization at both 80 and 130 °C, evidenced by measurements of proton conductivity in equilibrium with ethanol solution (Fig. 3).

Fig. 8 presents the *I*–*V* curves for the DEFC single cells based on Nafion-SiO_2 hybrid electrolytes with 6.5 and 13 wt% of SiO_2 and commercial PtSn/C anode catalyst at 80 °C and 130 °C. Overall, comparison with data shown in Fig. 7 indicates that the DEFCs based on Nafion-SiO_2 hybrids exhibit the same polarization profile than those with unmodified Nafion as electrolyte. A marked improvement of the performance for DEFC with Nafion-SiO_2 membranes is observed for both SiO_2 contents. For the hybrid membrane with 6.5 wt% of SiO_2, the polarization curve taken at 80 °C reached a maximum power density of 40 mW cm^{-2}, while for the DEFC operated at 130 °C the maximum power density was 61 mW cm^{-2}. These results are significantly superior (30 and 83%, respectively) to those obtained for unmodified Nafion 115 in the same conditions. For the hybrid with 13 wt% of SiO_2, the *I*–*V* curve measured at 80 °C reached a maximum power density of 37 mW cm^{-2}, which was increased to 62 mW cm^{-2} at 130 °C. In both cases, such an improved performance can be ascribed to the enhanced ionic conductivity in ethanol measured for the Nafion-SiO_2 hybrids (Fig. 3), as compared to Nafion. Results clearly reveal the important role of the hybrid membranes on the performance of the DEFC as the addition of silica allowed a significant performance enhancement with increasing operating temperature.

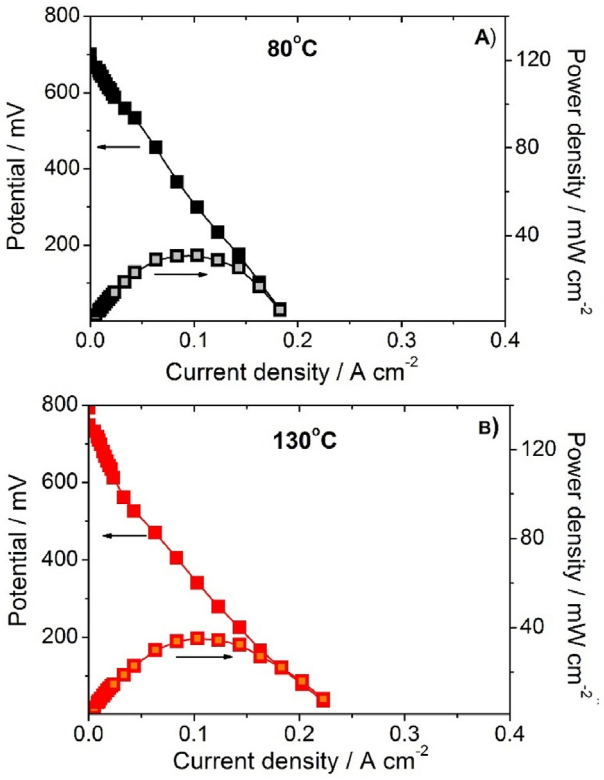

Fig. 7 – Polarization curves of DEFC prototypes using unmodified Nafion 115 as electrolyte and commercial PtSn/C as anode catalyst. 1.0 mg Pt cm^{-2} (anode and cathode). 2 mL min^{-1} flux of 2.0 mol L^{-1} ethanol solution fed at room temperature at A) 80 °C and B) 130 °C.

Table 2 – Results from the fitting the Pt $4f_{7/2}$ and Sn $3d_{5/2}$ XPS spectra of the homemade PtSn/C catalyst. Values in parentheses are the atomic percentage of each component.

	BE/eV and (at.%)	Assignment
Pt $4f_{7/2}$	71.9 (85)	Pt^0
	72.5 (12.5)	Pt^{2+} PtO, ($Pt(OH)_2$)
	74.4 (2.5)	Pt^{4+} (PtO_2; $PtO_2{\cdot}nH_2O$)
Sn $3d_{5/2}$	485.6 (38.7)	Sn^0
	487.3 (61.3)	Sn^{4+} and/or Sn^{2+} (SnO_2, SnO)

As discussed above, OCV values for measurements performed at 80 °C are inferior to those obtained at 130 °C for the same electrolyte, as shown in Table 3, where some previously reported data are included for comparison [60,61,63] despite the fact that they were obtained under different operating conditions from those used in this work. It is well known that the OCV of DEFCs is affected by ethanol crossover and, therefore, the higher OCV values serve as indication of the reduction of ethanol crossover at higher temperature, a clear beneficial effect of increasing the operating temperature of DEFC's devices. In fact, the ethanol fed to the DEFC at 130 °C is in vapor phase, which means that most of the ethanol reaching the anode interface in vapor form is likely to be less susceptible to permeation across the membrane. On the other hand, comparison of results obtained at the same operation temperature for DEFCs with Nafion-SiO_2 hybrids reveals that, although the particles of the inorganic filler could act as a physical barrier hindering alcohol crossover [26,31], the

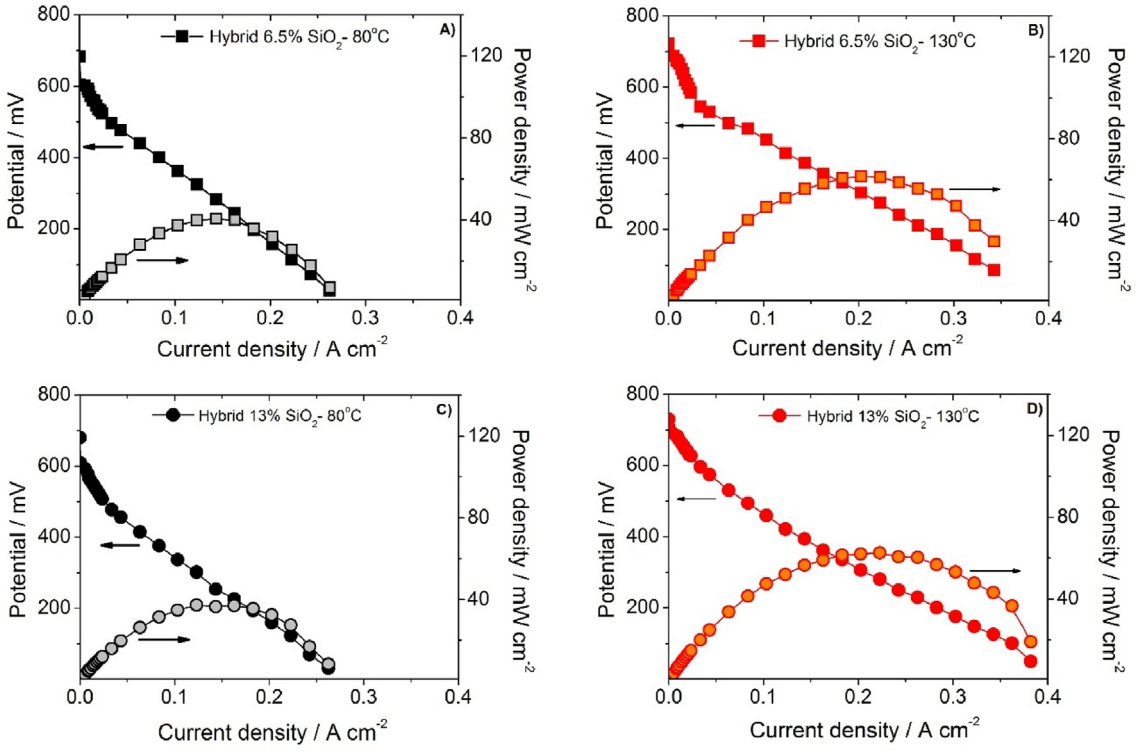

Fig. 8 – Polarization curves of DEFC prototypes at different temperatures for Nafion-SiO_2 hybrid electrolytes: 6.5 wt% SiO_2 (A and B); 13 wt% SiO_2 (C and D), A and C at 80 °C and B and C at 130 °C. Commercial PtSn/C anode. Electrodes with loading of 1.0 mg Pt cm^{-2} (anode and cathode) and 2 mL min^{-1} flux of 2.0 mol L^{-1} ethanol solution fed at room temperature.

Table 3 – Maximum power density and OCV values of DEFCs for Nafion and Nafion-SiO_2 hybrid membranes at different operation temperatures and ethanol fluxes. All values are the average for three independent samples. Commercial PtSn/C anode catalyst.

Membrane	Temperature (°C)	2 M Ethanol flux (mL min^{-1})	Maximum power density (mW cm^{-2})	OCV (mV)
N115	80	2	30 ± 2	700 ± 2
		5	45 ± 2	708 ± 2
		10	51 ± 3	712 ± 4
	130	2	35 ± 2	793 ± 2
		5	44 ± 3	791 ± 4
		10	58 ± 3	760 ± 4
Hybrid 6.5 wt% SiO_2	80	2	40 ± 1	683 ± 2
		5	40 ± 2	683 ± 2
		10	42 ± 3	687 ± 3
	130	2	61 ± 2	722 ± 4
		5	60 ± 2	683 ± 3
		10	64 ± 1	659 ± 3
Hybrid 13 wt% SiO_2	80	2	36 ± 3	681 ± 2
		5	36 ± 3	678 ± 2
		10	37 ± 2	680 ± 3
	130	2	61 ± 2	731 ± 4
		5	61 ± 1	755 ± 4
		10	62 ± 3	731 ± 3
Nafion 115	90	–	20	700 [57]
Nafion 115	90	–	38	750 [58]
Nafion 115	90	2	37	750 [62]

relatively low volume fraction of silica is possibly insufficient to ensure a significant reduction of the crossover [28].

Some additional measurements for DEFCs composed by a Nafion-SiO_2 hybrid electrolyte and a commercial PtSn/C anode catalyst were performed with ethanol solution flow rates of 5 and 10 mL min^{-1}. The polarization curves collected at 80 and 130 °C are presented in Figs. S3 and S4. In terms of OCV, no appreciable difference is observed for the Nafion-SiO_2 hybrids

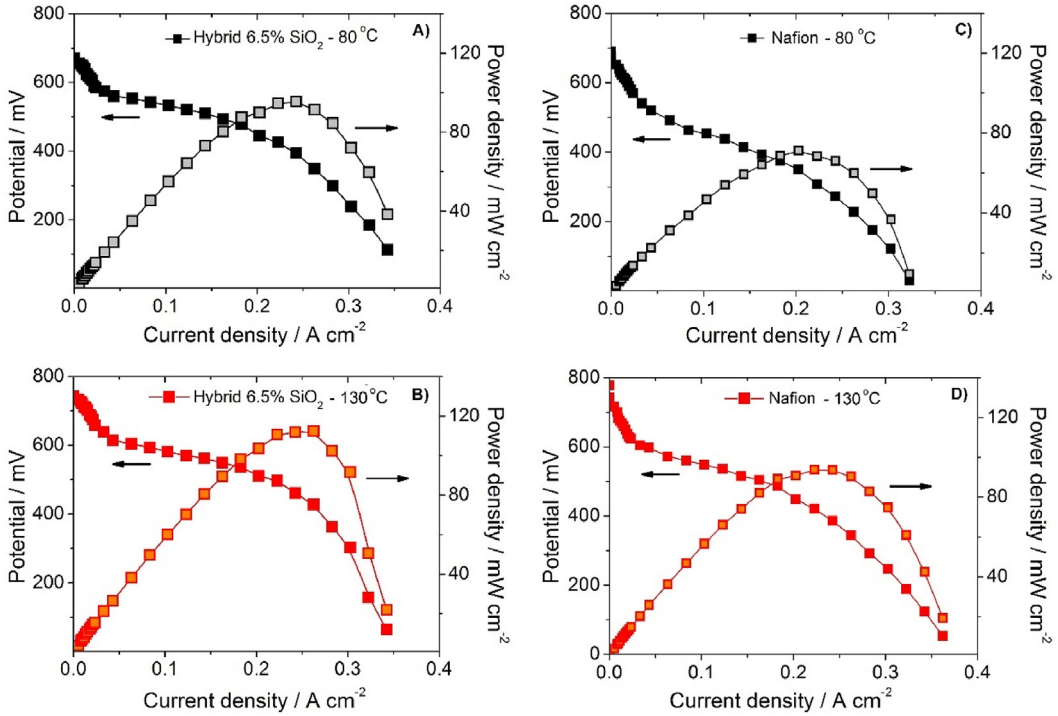

Fig. 9 – Polarization curves of DEFC prototypes with in-house prepared PtSn/C anode catalyst. A) Nafion-SiO_2 (6.5 wt% SiO_2) hybrid electrolyte at 80 °C, B) Nafion 115 at 80 °C, C) Nafion-SiO_2 (6.5 wt% SiO_2) hybrid electrolyte at 130 °C, D) Nafion 115 at 130 °C. Pt loading on both anode and cathode was 1.0 mg Pt cm^{-2} and 2 mL min^{-1} flux of 2.0 mol L^{-1} ethanol solution fed at room temperature.

at 80 °C, revealing that the 2.0 mol L^{-1} ethanol solution flow does not influence the ethanol solution crossover when hybrids are employed at low temperature. In contrast, at 130 °C, increasing the ethanol flow rate leads to a slight decrease in OCV values for both hybrids. These variations of OCV are consistent with the increase of crossover with temperature reported for Nafion membranes [64]. The possibility of additional effects on the OCV due to products of ethanol oxidation on the cathode catalyst, as well as crossover of acetaldehyde from the anode to the cathode compartment, were also discussed by some authors [65]. A rigorous analysis of these different contributions to the drop of OCV requires chemical analyses of reactants and products *in operando* and is beyond the scope of this study. On the other hand, Table 3 and Figs. S3 and S4 evidence that the maximum power densities for DEFCs operating at 80 °C and 130 °C are not affected by the ethanol flow rate, which can be explained keeping in mind that as current increases the ethanol depletion in the anode catalyst layer reduces the crossover to the cathode. Similar maximum power densities have been reported for PtSn/C-based catalysts and commercial Nafion below 90 °C, while at higher temperatures, DEFC performance seems to be quite dependent on the operational parameters and inherent characteristics of electrocatalysts and membranes, with large variation in terms of absolute maximum power density values [66].

The combination of the best-performing Nafion-SiO_2 (6.5 wt% SiO_2) and the in-house prepared PtSn/C as anode catalyst was tested in a DEFC prototype at 80 and 130 °C with ethanol solution flow rate of 2 mL min^{-1}. The *I*–*V* and power density curves are shown in Fig. 9, along with those obtained with Nafion 115 electrolyte. Independently of the electrolyte, enhanced performance is observed at 130 °C. However, at both measuring temperatures a remarkable increase of the maximum power density is evidenced for the DEFCs with Nafion-SiO_2 electrolytes as compared to those with Nafion 115.

Fig. 9 shows that the polarization profiles for the prototypes with Nafion-SiO_2 are quite similar at both operation temperatures, with a remarkable diminution of the ohmic drop overpotential associated to the hybrid membrane, which maintain the hydration and ensure H^+ conductance in water/ethanol mixture. Furthermore, it is possible to observe an unusual mass transport limiting polarization with a limit current of about 0.26 A cm^{-2} for both measured temperatures.

Comparison of the curves for DEFC with Nafion 115 electrolyte with those depicted in Fig. 7 provides clear evidence of the substantial enhancement of performance achieved by the substitution of the commercial anode catalyst by the home-made PtSn/C material, in which higher activity can be attributed to structural and morphological properties (smaller average particle size and polydispersity index) combined with a slightly larger degree of alloying. In particular, the enhanced activity promoted by the increase of alloyed Sn was previously observed for PtSn/C catalysts with the same composition and comparable particle sizes [55]. Previous published data have shown that fully alloyed Pt_3Sn catalysts have the highest activity for ethanol oxidation in acid environments [67]. The same conclusion was reached based on a simple model

employed to assess the contribution of alloyed and non-alloyed platinum and tin regarding the DEFC performance [68]. On the same line, other theoretical studies pointed out that alloyed structures might be an effective way of increasing activity towards ethanol oxidation [69].

As shown in Fig. 9, the maximum power density at 80 °C reached 95 mW cm^{-2} for the DEFC with hybrid electrolyte and homemade anode catalyst. This value of maximum power density represents a threefold increase with respect to those of Figs. 6a and 7a for DEFCs using commercial PtSn/C catalyst and both the unmodified Nafion and the Nafion-SiO_2 (6.5 wt%). However, a striking performance enhancement was observed by increasing the operating temperature of DEFC to 130 °C. The DEFC with hybrid electrolyte and optimized electrocatalyst exhibited a maximum power density of 112 mW cm^{-2}, which demonstrates that DEFC performance can be substantially improved by the combined effects of optimized electrolyte and electrocatalyst.

It is noteworthy that the maximum power densities of the DEFC with Nafion-SiO_2 (6.5 wt%) electrolyte and homemade PtSn/C anode catalyst are higher than most values reported for DEFCs with PtSn anode catalysts. Even though some higher values were reported for somewhat different conditions and membrane-catalysts combinations, the results reported herein show that development of membranes with better hygroscopic properties and more active catalysts combined with high temperature operation is a promising route to further improvements of DEFCs performance.

Conclusions

Nafion-SiO_2 hybrids with two different contents of SiO_2 (6.5 and 13 wt%) incorporated in the Nafion polymeric matrix were prepared employing different TEOS concentrations during the sol-gel synthesis. The uptake values for water and ethanol solution demonstrate the improved hygroscopic properties of the hybrids compared with Nafion. The hybrid membranes exhibit higher thermal stability as inferred from DSC scans. Proton conductivity measurements clearly indicate that the Nafion-SiO_2 hybrid with lower SiO_2 content presents better proton conductivity than unmodified Nafion in the whole temperature range analyzed. More important for DEFC tests, hybrid electrolytes displayed considerably higher proton conductivity than Nafion in ethanol solution, a feature more marked at high measuring temperatures. The DEFC polarization curves of prototypes using Nafion-SiO_2 hybrid electrolytes showed improved performance in comparison with that with unmodified Nafion, which can be understood in terms of the higher proton conductivity of the hybrid electrolytes promoted by the hygroscopic characteristics of the SiO_2 filler. DEFC data obtained in this work at 80 °C and 130 °C demonstrate that the performance enhancement is not directly related to the SiO_2 content. Nevertheless, both hybrids performed better than Nafion.

DEFC shows substantial differences in performance depending on the PtSn/C anode catalysts. The homemade PtSn/C anode presents a substantially superior performance than the commercial catalyst. The combination of the hybrid electrolyte with the highly active in-house prepared PtSn/C catalyst leads to a largely improved polarization performance, with a maximum power density of 112 mW cm^{-2} at 130 °C. The experimental results presented herein demonstrate the benefits of combining optimized component materials to open up new possibilities for improving the performance of DEFCs.

Declaration of competing interest

The authors declare that they have no known competing financial interests or personal relationships that could have appeared to influence the work reported in this paper.

Acknowledgments

This research was funded by Shell (ANP) and The São Paulo Research Foundation (FAPESP) [2017/11937-4] as part of Center For Innovation on New Energies (CINE). This work was also partially funded by FAPESP [2014/09087-4, 2014/50279-4, 2014/12255-6], CAPES and CNEN. FCF, EIS and HMV are CNPq fellows. Thanks are due to Dr. A. B. Lugão and MSc. H. A. Zen (Instituto de Pesquisas Energéticas e Nucleares - IPEN/CNEN) for helping us with DSC measurements and to Dr. Emilia A. Carbonio (Helmholtz-Zentrum Berlin für Materialien und Energie, Germany) for valuable discussions on XPS data treatment. The authors also thank the Laboratory of Structural Characterization (LCE/DEMa/UFSCar) for the general facilities.

Appendix A. Supplementary data

Supplementary data to this article can be found online at https://doi.org/10.1016/j.ijhydene.2021.01.123.

REFERENCES

[1] Srinivasan S, Mosdale R, Stevens P, Yang C. Fuel cells: reaching the era of clean and efficient power generation in the twenty-first century. Annu Rev Energy Environ 1999;24:281.
[2] Kamarudin MZF, Kamarudin SK, Masdar MS, Daud WRW. Review: direct ethanol fuel cells. Int J Hydrogen Energy 2013;38:9438.
[3] Da Silva AAA, Steil MC, Tabuti FN, Rabelo-Neto RC, Noronha FB, Mattos LV, Fonseca FC. The role of the ceria dopant on NI/doped-ceria anodic layer cermets for direct ethanol solid oxide fuel cell. Int J Hydrogen Energy 2021;46:4309.
[4] Ju H, Badwal S, Giddey S. A comprehensive review of carb on and hydrocarbon assisted water electrolysis for hydrogen production. Appl Energy 2018;231:502.
[5] de Salvo Junior O, de Almeida FGV. Influence of technologies on energy efficiency results of official Brazilian tests of vehicle energy consumption. Appl Energy 2019;241:98.
[6] Linzenich A, Arning K, Bongartz D, Mitsos A, Ziefle M. What fuels the adoption of alternative fuels? Examining preferences of German car drives for fuel innovations. Appl Energy 2019;249:222.

[7] Badwal SPS, Giddey S, Kulkarni A, Goel J, Basu S. Direct ethanol fuel cells for transport and stationary applications – a comprehensive review. Appl Energy 2015;145:80.
[8] Zhao TS, Li YS, Shen SY. Anion-exchange membrane direct ethanol fuel cells: status and perspective. Front Energy Power Eng China 2010;4:443.
[9] Zhao Y, Damgaard A, Xu Y, Liu S, Christensen TH. Bioethanol from corn stover – global warming footprint of alternative biotechnologies. Appl Energy 2019;247:237.
[10] Akhairi MAF, Kamarudin SK. Catalysts in direct ethanol fuel cell (DEFC): an overview. Int J Hydrogen Energy 2016;41:4214.
[11] Choudhary AK, Pramanik H. Enhancement of ethanol electrooxidation in half cell and single direct ethanol fuel cell (DEFC) using post-treated polyol synthesized Pt-Ru nano electrocatalysts supported on HNO_3-functionalized acetylene black carbon. Int J Hydrogen Energy 2020;45:574.
[12] Ahmed Z, Matos BR, Florio DZ, Rey JFQ, Santiago EI, Fonseca FC. Nafion-mesoporous silica composite electrolyte: properties and direct ethanol fuel cells performance. Mater Renew Sustain Energy 2016;5(6):1.
[13] Uchida H, Izumi K, Aoki K, Watanabe M. Temperature-dependence of hydrogen oxidation reaction rates and CO-tolerance at carbon-supported Pt, Pt–Co, and Pt–Ru catalysts. Phys Chem Chem Phys 2009;11:1771.
[14] Bach Delpeuch A, Asset T, Chatenet M, Cremers C. Influence of the temperature for the ethanol oxidation reaction (EOR) on Pt/C, Pt-Rh/C and Pt-Rh-SnO_2/C. Fuel Cell 2015;15:352–60.
[15] Mauritz KA, Moore RB. State of understanding of nafion. Chem Rev 2004;104:4535.
[16] Pourzare K, Mansourpanah Y, Farhadi S. Advanced nanocomposite membranes for fuel cell applications: a comprehensive review. Biofuel Res J 2016;3:496.
[17] Quartarone E, Angioni S, Mustarelli P. Polymer and composite membranes for proton-conducting, high-temperature fuel cells: a critical review. Materials 2017:10.
[18] Subianto S. Recent advances in polybenzimidazole/phosphoric acid membranes for high-temperature fuel cells. Polym Int 2014;63:1134.
[19] Araya SS, Zhou F, Liso V, Sahlin SL, Vang JR, Thomas S, Gao X, Jeppesen C, Kær SK. Comprehensive review of PBI-based high temperature PEM fuel cells. Int J Hydrogen Energy 2016;41:21310.
[20] Haque MA, Sulong AB, Loh KS, Majlan EH, Husaini T, Rosli RE. Acid doped polybenzimidazoles based membrane electrode assembly for high temperature proton exchange membrane fuel cell: a review. Int J Hydrogen Energy 2017;42:9156.
[21] Amjadi M, Rowshanzamir S, Peighambardoust SJ, Hosseini MG, Eikani MH. Investigation of physical properties and cell performance of Nafion/TiO_2 nanocomposite membranes for high temperature PEM fuel cells. Int J Hydrogen Energy 2010;35:9252.
[22] Santiago EI, Isidoro RA, Dresch MA, Matos BR, Linardi M, Fonseca FC. Nafion-TiO_2 hybrid electrolytes for stable operation of PEM fuel cells at high temperature, Electrochim. Acta 2009;54:4111.
[23] Dresch MA, Isidoro RA, Linardi M, Rey JFQ, Fonseca FC, Santiago EI. Influence of sol-gel media on the properties of Nafion-SiO_2 hybrid electrolytes for high performance proton exchange membrane fuel cells operating at high temperature and low humidity. Electrochim Acta 2013;94:353.
[24] Ying YP, Kamarudin SK, Masdar MS. Silica-related membranes in fuel cell applications: an overview. Int J Hydrogen Energy 2018;43:16068.
[25] Karimi MB, Mohammadi F, Hooshyari K. Recent approaches to improve Nafion performance for fuel cell applications: a review. Int J Hydrogen Energy 2019;44:28919.
[26] Ahmed Z, Matos BR, de Florio DZ, Rey JFQ, Santiago EI, Fonseca FC. Nafion-mesoporous silica composite electrolyte: properties and direct ethanol fuel cells performance. J Renew Sustain Energy 2016;5:6.
[27] Matos BR, Isidoro RA, Santiago EI, Tavares AC, Ferlauto AS, Muccillo R, Fonseca FC. Nafion-titanate nanotubes composites prepared by in situ crystallization and casting for direct ethanol fuel cells. Int J Hydrogen Energy 2015;40:1859.
[28] Matos BR, Isidoro RA, Santiago EI, Fonseca FC. Performance enhancement of direct ethanol fuel cell using Nafion composites with high volume fraction of titania. J Power Sources 2014;268:706.
[29] Barbora L, Acharya S, Verma A. Synthesis and ex-situ characterization of nafion/TiO_2 composite membranes for direct ethanol fuel cell. Macromol Symp 2009;277:177.
[30] Dresch MA, Matos BR, Fonseca FC, Santiago EI, Carmo M, Lanfredi AJC, Balog S. Small-angle X-ray and neutron scattering study of Nafion-SiO_2 hybrid membranes prepared in different solvent media. J Power Sources 2015;274:560.
[31] Matos BR, Santiago EI, Rey JFQ, Ferlauto AS, Traversa E, Linardi M, Fonseca FC. Nafion-based composite electrolytes for proton exchange membrane fuel cells operating above 120°C with titania nanoparticles and nanotubes as fillers. J Power Sources 2011;196:1061.
[32] Antolini E. Catalysts for direct ethanol fuel cells. J Power Sources 2007;170:1.
[33] Beyhan S, Coutanceau C, Leger JM, Napporn TW, Kadirgan F. Promising anode candidates for direct ethanol fuel cell: carbon supported PtSn-based trimetallic catalysts prepared by Bonnemann method. Int J Hydrogen Energy 2013;38:6830.
[34] Rousseau S, Coutanceau C, Lamy C, Leger JM. Direct ethanol fuel cell (DEFC): electrical performances and reaction products distribution under operating conditions with different platinum-based anodes. J Power Sources 2006;158:18.
[35] Vigier F, Rousseau S, Coutanceau C, Leger JM, Lamy C. Electrocatalysis for the direct alcohol fuel cell. Top Catal 2006;40:111.
[36] Linares JJ, Rocha TA, Zignani S, Paganin VA, Gonzalez ER. Different anode catalyst for high temperature polybenzimidazole-based direct ethanol fuel cells. Int J Hydrogen Energy 2013;38:620.
[37] Zhou Y, Xu QJ. A review of Pt-based anode catalysts preparation for direct ethanol fuel cell. Adv Mater Res 2014;860–863:797.
[38] Ma KB, Han SB, Kwon SH, Kwak DH, Park KW. High-performance direct ethanol fuel cell using nitrate reduction reaction. Int J Hydrogen Energy 2018;43:17265.
[39] Colmati F, Magalhães MM, Sousa Jr R, Ciapina EG, Gonzalez ER. Direct Ethanol Fuel Cells: the influence of structural and electronic effects on Pt-Sn/C electrocatalysts. Int J Hydrogen Energy 2019;44:28812.
[40] Matos BR, Santiago EI, Rey JFQ, Scuracchio CH, Mantovani GL, Hirano LA, Fonseca FC. *Dc* Proton conductivity at low-frequency in Nafion conductivity spectrum probed by time-resolved SAXS measurements and impedance spectroscopy. J Polym Sci B Polym Phys 2015;53:822.
[41] Santiago EI, Varanda LC, Villullas HM. Carbon-supported Pt-Co catalysts prepared by a modifled polyol process as cathodes for PEM fuel cells. J Phys Chem C 2007;111:3146.
[42] Varanda LC, Jafelicci M. Self-assembled FePt nanocrystals with large coercivity: reduction of the fcc-to-L1(0) ordering temperature. J Am Chem Soc 2006;128:11062.
[43] Paganin VA, Ticianelli EA, Gonzalez ER. Development and electrochemical studies of gas diffusion electrodes for polymer electrolyte fuel cells. J Appl Electrochem 1996;26:297.

[44] Matos BR, da Silva JS, Santiago EI, Parra DF, Carastan DJ, de Florio DZ, Andrada HE, Carreras AC, Fonseca FC. Proton and cesium conductivity in perfluorosulfonate ionomers at low and high relative humidity. Solid State Ionics 2017;301:86.
[45] Matos BR, Santiago EI, Muccillo R, Velasco-Davalos IA, Ruediger A, Tavares AC, Fonseca FC. Interplay between α-relaxation and morphology transition of perfluorosulfonate ionomer membranes. J Power Sources 2015;293:859.
[46] Liu C, Bonaccurso E, Butt H-J. Evaporation of sessile water/ethanol drops in a controlled environment. Phys Chem Chem Phys 2008;10:7150.
[47] Rowan SM, Newton MI, Driewer FW, McHale G. Evaporation of microdroplets of azeotropic liquids. J Phys Chem B 2000;104:8217.
[48] Baturina OA, Aubuchon SR, Wynne KJ. Thermal stability in air of Pt/C catalysts and PEM fuel cell catalyst layers. Chem Mater 2006;18:1498.
[49] Cullity BC. Elements of X-ray diffraction. 2nd ed. London: Addison-Wesley Publishing Company, Inc.; 1978.
[50] Antolini E, Colmati F, Gonzalez ER. Ethanol oxidation on carbon supported (PtSn)(alloy)/SnO_2 and (PtSnPd)(alloy)/SnO_2 catalysts with a fixed Pt/SnO_2 atomic ratio: effect of the alloy phase characteristics. J Power Sources 2009;193:555.
[51] Durussel Ph, Massara R, Feschotte P. Le système binaire Pt-Sn. J Alloys Compd 1994;215:175.
[52] Hoheisel M, Speller S, Kuntze J, Atrei A, Bardi U, Heiland W. Structure Pt_3Sn(110) studied by scanning tunneling microscopy. Phys Rev B 2001;63:245403.
[53] Colmati F, Antolini E, Gonzalez ER. Effect of temperature on the mechanism of ethanol oxidation on carbon supported Pt, PtRu and Pt_3Sn electrocatalysts. J Power Sources 2006;157:98.
[54] Hunter RJ. Foundations of colloid science. Oxford: Clarendon Press; 1989.
[55] Hüfner S. Photoelectron spectroscopy: principles and applications. Berlin: Springer Verlag; 2003.
[56] Doniach S, Sunjic M. Many-electron singularity in X-ray photoemission and X-ray line spectra from metals. J Phys C Solid State Phys 1970;3:285.
[57] Hüfner S, Wertheim GK, Wernick JH. XPS core line asymmetrics in metals. Solid State Commun 1975;17:417.
[58] Keister JW, Rowe JE, Kolodziej JJ, Madey TE. Photoemission spectroscopy of platinum overlayers on silicon dioxide films. J Vac Sci Technol B 2000;18:2174.
[59] Godoi DRM, Perez J, Villullas HM. Alloys and oxides on carbon-supported Pt-Sn electrocatalysts for ethanol oxidation. J Power Sources 2010;195:3394.
[60] Colmati F, Antolini E, Gonzalez ER. Ethanol oxidation on a carbon-supported Pt75Sn25 electrocatalyst prepared by reduction with formic acid: effect of thermal treatment. Appl Catal B Environ 2007;73:106.
[61] Zignani SC, Baglio V, Gonzalez ER, Aricò AS. Durability of a PtSn ethanol oxidation electrocatalyst. ChemElectroChem 2014;1:1403.
[62] Larminie J, Dicks A. Fuel cell systems explained. 2a. edition. John Wiley & Sons Inc.; 2003.
[63] Purgato FLS, Pronier S, Olivi P, de Andrade AR, Leger JM, Tremiliosi-Filho G, Kokoh KB. Direct ethanol fuel cell: electrochemical performance at 90 degrees C on Pt and PtSn/C electrocatalysts. J Power Sources 2012;198:95.
[64] Kontou S, Stergiopoulos V, Song S, Tsiakaras P. Ethanol/water mixture permeation through a Nafion (R) based membrane electrode assembly. J Power Sources 2007;171:1.
[65] Suresh NS, Jayanti S. Cross-over and performance modeling of liquid-feed polymer electrolyte membrane direct ethanol fuel cells. Int J Hydrogen Energy 2011;36:14648.
[66] Azam AMIN, Lee SH, Masdar MS, Zainoodin AM, Kamarudin SK. Int J Hydrogen Energy 2019;44:8566.
[67] Antolini E, Gonzalez ER. Effect of synthesis method and structural characteristics of Pt-Sn fuel cell catalysts on the electro-oxidation of CH_3OH and CH_3CH_2OH in acid medium. Catal Today 2011;160:28.
[68] Antolini E, Gonzalez ER. A simple model to assess the contribution of alloyed and non-alloyed platinum and tin to the ethanol oxidation reaction on Pt-Sn/C catalysts: application to direct ethanol fuel cell performance. Electrochim Acta 2010;55:6485.
[69] An W, Men Y, Wang JG, Liu P. Interfacial and alloying effects on activation of ethanol from first-principles. J Phys Chem C 2017;121:5603.
[70] Matos BR. The genuine ac-to-dc proton conductivity crossover of Nafion and polymer dielectric relaxations as a fuel cell polarization loss. J. Electroanal Chem 2020;871:114357. https://doi.org/10.1016/j.jelechem.2020.114357.